Maximum speed of dewetting on a fiber

Tak Shing Chan, Thomas Gueudré, and Jacco H. Snoeijer

Citation: Phys. Fluids **23**, 112103 (2011); doi: 10.1063/1.3659018
View online: http://dx.doi.org/10.1063/1.3659018
View Table of Contents: http://pof.aip.org/resource/1/PHFLE6/v23/i11
Published by the American Institute of Physics.

Maximum speed of dewetting on a fiber

Tak Shing Chan, Thomas Gueudré, and Jacco H. Snoeijer
Physics of Fluids Group and J. M. Burgers Centre for Fluid Dynamics, University of Twente, P.O. Box 217, 7500 AE Enschede, The Netherlands

(Received 1 June 2011; accepted 14 October 2011; published online 11 November 2011)

A solid object can be coated by a nonwetting liquid since a receding contact line cannot exceed a critical speed. We theoretically investigate this forced wetting transition for axisymmetric menisci on fibers of varying radii. First, we use a matched asymptotic expansion and derive the maximum speed of dewetting. For all radii, we find the maximum speed occurs at vanishing apparent contact angle. To further investigate the transition, we numerically determine the bifurcation diagram for steady menisci. It is found that the meniscus profiles on thick fibers are smooth, even when there is a film deposited between the bath and the contact line, while profiles on thin fibers exhibit strong oscillations. We discuss how this could lead to different experimental scenarios of film deposition.
 [doi:10.1063/1.3659018]

I. INTRODUCTION

A convenient way to deposit a thin liquid layer on a surface is by withdrawing a solid from a liquid reservoir. The film is dragged along with the solid due to the viscous friction of the liquid. This principle is known as dip-coating and is a commonly used technique in industrial contexts.[1,2] Once deposited on the surface, the film often has a thickness as predicted by Landau and Levich[3] and Deryaguin,[4] scaling with speed U of withdrawal as $h \propto U^{2/3}$. Recently, however, a different class of solutions were identified, which are much thicker and scale as $h \propto U^{1/2}$.[5] These thick films were indeed realized experimentally in the case where the solid was partially wetting.

The conditions of partial wetting introduce another interesting feature, namely that the film entrainment only appears above a critical velocity of withdrawal.[6–10] Below this speed, the contact line finds at a steady position, indicated as the meniscus rise Δ (Fig. 1). Due to viscous drag between the liquid and the solid, the dynamical position of Δ is higher than at equilibrium. This means that the apparent contact angle θ_{ap} of the dynamical meniscus is smaller than the equilibrium angle θ_e. The simplest interpretation of the transition to film deposition is that the apparent contact angle $\theta_{ap} \to 0$ at some critical plate velocity. This idea was already postulated by Deryaguin and Levi,[11] although the energy argument given by de Gennes[8] suggested a nonzero θ_{ap} at the transition. The hypothesis of $\theta_{ap} = 0$, however, was given a rigorous mathematical basis (for a flat solid) by asymptotic expansions of the lubrication equations.[12,13] Actually, it was shown by Ref. 10 that de Gennes energy argument can be extended to incorporate interface curvature: this exactly gives the lubrication equation, meaning that also the energy argument leads to a zero θ_{ap} at the transition. This theory gives a simple prediction for the maximum rise based on the static meniscus solution with vanishing contact angle—for a fiber of radius r_0, this simply becomes[14,15]

$$\Delta_{\max} \simeq \begin{cases} r_0\left(\ln\frac{4\ell_c}{r_0} - c\right) & \text{for } r_0 \ll \ell_c \\ \sqrt{2}\ell_c & \text{for } r_0 \gg \ell_c. \end{cases} \quad (1)$$

Here, $\ell_c = (\gamma/\rho g)^{1/2}$ is the capillary length based on surface tension γ, density ρ, and gravity g and c is Euler's constant (0.57721). At intermediate radii $r_0 \sim \ell_c$, the maximum rise can be determined numerically.

Experimentally, the description of the forced wetting transition has remained ambiguous. The condition of a vanishing apparent contact angle was convincingly shown by Sedev and Petrov.[16] When withdrawing fibers or thin cylinders ($r_0/\ell_c \sim 0.06 - 1$), they found a maximum rise of the meniscus consistent with Eq. (1). Using cylinders of larger radii ($r_0/\ell_c \sim 10$), Maleki *et al.*[17] found zero or nonzero θ_{ap} at the transition, depending on the way θ_{ap} was determined. When using the criterion based on the meniscus height, the transition was found slightly before reaching $\Delta_{\max}$. Yet another set of experiments using a flat plate ($r_0/\ell_c = \infty$) displayed a transition to film deposition clearly before reaching the maximum rise.[18,19] Still, during the unsteady entrainment phase, the maximum recorded speed was reached exactly at $\sqrt{2}\ell_c$. Note that in these experiments, the deposited liquid was not simply the Landau-Levich-Deryaguin film, but gave rise to thick films and even shock solutions. It was argued that the presence of these dynamical solutions are related to the pre-critical onset of entrainment,[20] but an explanation is still lacking.

An additional complexity is that the contact line can spontaneously develop sharp corner structures or even zig-zags. This has been observed in dip-coating,[21] splashing,[22] immersion lithography,[23,24] and for drops sliding down an inclined plane.[25,26] The conical structure of the interface near the contact line renders the problem truly three-dimensional, which affects the balance of the capillary forces.[27] For sliding drops, it has been observed experimentally and described by a 3D lubrication model that this change in geometry indeed leads to a nonzero apparent contact angle at the transition to liquid deposition.[28,29] This raises the question of how the geometry of the flow can influence the critical speed of wetting.[30]

In this paper, we theoretically study the withdrawal of fibers of arbitrary radii. By varying the ratio r_0/ℓ_c, we continuously

cover the range from thin fibers to the flat plate. First, we extend the asymptotic analysis that was previously done for the flat plate[12,13] to the limit of thin fibers (Sec. II). To resolve the singularity of viscous stress near the contact line,[31,32] we introduce a slip length λ.[33,34] Other types of microscopic regularization will give similar results.[10] Typical values for the slip and capillary lengths are $\lambda \sim 10^{-9}$ m and $\ell_c \sim 10^{-3}$ m, respectively. We can thus exploit the hierarchy of length scales

$$\lambda \ll r_0 \ll \ell_c, \tag{2}$$

and perform a matched asymptotic expansion. The control parameter is the capillary number $\mathrm{Ca} = U_0\eta/\gamma$, which is the speed of withdrawal scaled by viscosity η and surface tension γ. The analysis yields the critical capillary number, which depends on the value of r_0, and confirms that the maximum speed coincides with $\theta_{ap} = 0$, for all fiber radii r_0. In this sense, the change in geometry does not qualitatively change the nature of the critical point. However, striking differences do show up when computing numerically the complete bifurcation diagrams for all steady solutions (Sec. III). These diagrams include solution branches above $\Delta_{\max}$ that are unstable, but which have been observed as transients during film deposition for the plate case.[19] We find that for small fiber radii much below ℓ_c, the steady solutions no longer smoothly join the film solutions that mediate the deposition. In the Discussion (Sec. IV), we speculate that this is why, experimentally, it is easier to approach the critical point for thin fibers (Sec. IV).

II. ASYMPTOTIC ANALYSIS

We compute the shape of an axisymmetric meniscus on a fiber of radius r_0 using the method of matched asymptotic expansions. The interface is characterized by $h(x)$, as sketched in Fig. 1. The matching procedure is outlined schematically in Fig. 2. At small scales, the dominant balance is between viscosity η and surface tension γ and is characterized by the capillary number Ca. Viscous effects can be neglected on large scales, for which the interface profile is

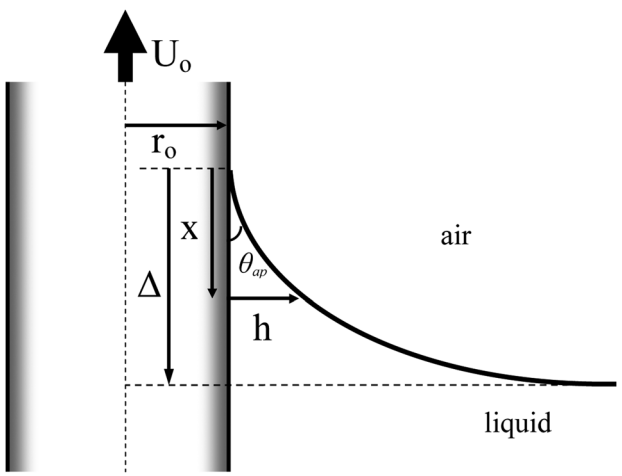

FIG. 1. Schematic representation of the dip-coating setup: A fiber or cylinder of radius r_0 is withdrawn with speed U_0 from a bath of viscous liquid. The axisymmetric meniscus profile is characterized by $h(x)$, while Δ denotes the maximum rise above the reservoir.

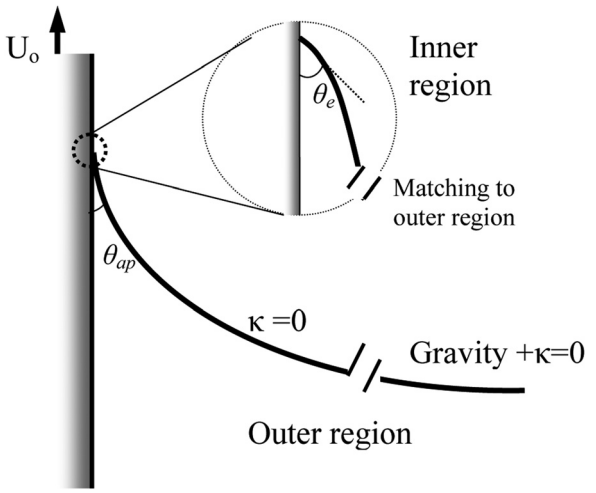

FIG. 2. Schematic diagram showing the different asymptotic regions for the case of a thin fiber. The inner region originates from a balance between viscosity and surface tension. It has a microscopic contact angle θ_e. The outer region is a static meniscus joining a fiber with an apparent contact angle θ_{ap}. When the fiber radius $r_0 \ll \ell_c$, the outer profile is further separated into two regions.[15]

that of a static meniscus. The problem is closed by matching the inner and outer solutions. The analysis provides the meniscus rise Δ as a function of Ca as well as the critical speed, both of which can be observed experimentally. We consider both large fiber radii $(r_0 \gg \ell_c)$ and small fiber radii $(r_0 \ll \ell_c)$. In all cases, we take r_0 and ℓ_c to be macroscopic and much greater than the microscopic cutoff. Throughout the analysis, we scale all lengths by the capillary length, i.e., $\ell_c = 1$.

A. Inner solution: Lubrication approximation

To distinguish the solution h in the inner region and the outer region, we denote $h_{in}(x)$ as the solution in inner region and $h_{out}(x)$ as the solution in outer region. The characteristic length scale for the inner solution comes from the cutoff of the viscous singularity, which here we take the slip length λ. Since typical interface curvatures turn out $\sim \mathrm{Ca}^{1/3}/\lambda$, as can be observed from the rescalings below, we can neglect the curvature contribution due to axisymmetry, which is of order $1/r_0$. Hence, for the inner solution, we can follow the analysis by Eggers,[12,13] which was originally derived for the flat plate. For completeness, we briefly summarize the analysis and the central results.

By restricting the analysis to small contact angles, $h'_{in}(0) = \theta_e \ll 1$, one can determine $h(x)$ from the lubrication approximation:[35]

$$h'''_{in} = \frac{3\mathrm{Ca}}{h_{in}^2 + 3\lambda h_{in}}. \tag{3}$$

Since the slip length λ is the only length scale, we rescale the solutions according to

$$h_{in}(x) = 3\lambda H\left(\frac{x\theta_e}{3\lambda}\right), \quad \xi = \frac{x\theta_e}{3\lambda}. \tag{4}$$

Hence, Eq. (4) reduces to

$$H''' = \frac{\delta}{H^2 + H}, \tag{5}$$

where we introduced a reduced capillary number $\delta = 3\mathrm{Ca}/\theta_e^3$. The boundary conditions are

$$H(\xi = 0) = 0, \tag{6}$$

$$H'(\xi = 0) = 1, \tag{7}$$

and the asymptotic behavior that has to be matched to the outer solution. Away from the contact line, where $H \gg 1$, Eq. (5) further reduces to

$$y''' = \frac{1}{y^2}, \tag{8}$$

where we have put $H(\xi) = \delta^{1/3} y(\xi)$. This equation has an exact solution, whose properties have been summarized in Ref. 36. In parametric form, a solution with $y(0) = 0$ reads

$$\left.\begin{aligned} \xi &= \frac{2^{1/3}\pi Ai(s)}{\beta(\alpha Ai(s) + \beta Bi(s))} \\ y &= \frac{1}{(\alpha Ai(s) + \beta Bi(s))^2} \end{aligned}\right\} s \in [s_1, \infty[, \tag{9}$$

where Ai and Bi are Airy functions.[37] The limit $\xi \to 0$ corresponds to $s \to \infty$, the opposite limit $\xi \to \infty$ to $s \to s_1$, where s_1 is a root of the denominator of Eq. (9)

$$\alpha Ai(s_1) + \beta Bi(s_1) = 0. \tag{10}$$

Since the solution extends to $s = \infty$, s_1 has to be the largest root of Eq. (10).

The solution $y(\xi)$ is thus characterized by three parameters α, β, and s_1. Note that these are related according to Eq. (10), so that only two parameters are independent. The constant β can be determined by matching Eq. (9), which is valid only for $\xi \gtrsim 1$, to a solution of Eq. (5), which includes the effect of the cutoff and is thus valid down to the position $\xi = 0$ of the contact line.[13] It was found that

$$\beta^2 = \pi \exp(-1/(3\delta))/2^{2/3} + O(\delta), \tag{11}$$

which eliminates one of the two free parameters. The remaining parameter will be eliminated below by matching the large scale asymptotics of $y(\xi)$ the outer solution of the problem. For that, we only need the asymptotic behavior of $y(\xi)$ for large ξ, which reads

$$y(\xi) = \frac{1}{2}\kappa_y \xi^2 + b_y \xi + \mathcal{O}(1), \tag{12}$$

where

$$\kappa_y = \left(\frac{2^{1/6}\beta}{\pi Ai(s_1)}\right)^2, \quad b_y = \frac{-2^{2/3} Ai'(s_1)}{Ai(s_1)}. \tag{13}$$

B. Outer solution: Static meniscus

At the scale of outer solution, one can neglect viscous effects and the profile is governed by surface tension and gravity. Thus, equating the hydrostatic pressure and the capillary pressure gives

$$\kappa = \Delta - x, \tag{14}$$

where κ is the curvature of the interface. Remind that we expressed all lengths in the capillary length $\ell_c = 1$. The curvature can be expressed from the geometric relation

$$\kappa = \frac{h''_{\mathrm{out}}}{(1 + h'^2_{\mathrm{out}})^{3/2}} - \frac{1}{(r_0 + h_{\mathrm{out}})(1 + h'^2_{\mathrm{out}})^{1/2}}. \tag{15}$$

The corresponding outer solution $h_{out}(x)$ is that of a meniscus of a liquid reservoir joining the fiber surface. The contact angle of the meniscus at the surface is denoted as the apparent contact angle, θ_{ap}, since it refers to the apparent angle on the scale of the outer solution. The boundary conditions, therefore, are

$$h_{\mathrm{out}}(x = 0) = 0, \tag{16}$$

$$h'_{\mathrm{out}}(x = 0) = \theta_{ap}, \tag{17}$$

$$h'_{\mathrm{out}}(x = \Delta) = \infty. \tag{18}$$

For the present analysis, we require only the asymptotic behavior near the contact line, which is obtained by a Taylor expansion,

$$h_{\mathrm{out}}(x) = \theta_{ap} x + \frac{1}{2}\kappa_{ap} x^2 + \mathcal{O}(x^3). \tag{19}$$

Note that, we consider small θ_{ap}, since the inner solution is obtained in the lubrication limit.

In general, the governing Eq. (14) cannot be solved analytically. In the following, we will consider two extreme cases for which analytical solution can be obtained, namely the larger fiber radius case ($r_0 \gg 1$) and the small fiber radius case ($r_0 \ll 1$).

1. Large fiber radius: $r_0 \gg 1$

In the case where the fiber radius is much larger than the capillary length, the second term on the right hand side of Eq. (15) due to the curvature of the fiber can be neglected. Then, Eq. (14) can be written as

$$\frac{h''_{\mathrm{out}}}{(1 + h'^2_{\mathrm{out}})^{3/2}} = \Delta - x. \tag{20}$$

Integrating Eq. (20) once with respect to x, we obtain

$$1 - \frac{h'_{\mathrm{out}}}{(1 + h'^2_{\mathrm{out}})^{1/2}} = \frac{1}{2}(\Delta - x)^2, \tag{21}$$

where the boundary condition $h'_{\mathrm{out}} \to \infty$ at the position of the reservoir ($x = \Delta$) is used. Evaluating Eq. (21) at the contact line position ($x = 0$) and using the geometrical connection $\sin\theta = h'_{\mathrm{out}}/\sqrt{1 + h'^2_{\mathrm{out}}}$, we end up with

$$\Delta = \sqrt{2(1 - \sin\theta_{ap})}, \tag{22}$$

$$\simeq \sqrt{2}(1 - \theta_{ap}/2), \tag{23}$$

and Eq. (14) immediately gives

$$\kappa_{ap} \simeq \sqrt{2}(1-\theta_{ap}/2). \tag{24}$$

2. Small fiber radius: $r_0 \ll 1$

For thin fibers, it has been shown that the outer region can be further divided into two subregions,[15] as has been sketched in Fig. 2. In the region far away from the fiber ($h \gg 1$), the term due to the curvature of the fiber can be neglected. On the other hand, gravity can be neglected in the region close to the fiber ($h \ll 1$), and the meniscus is determined by the balance between the two curvature terms in Eq. (15). The profile near the fiber is a classical zero curvature interface that can be expressed as

$$h_{\text{out}}(x) = r_0\left[\cosh\left(\frac{x}{r_0\cos\theta_{ap}}\right) + \sin\theta_{ap}\sinh\left(\frac{x}{r_0\cos\theta_{ap}}\right) - 1\right]. \tag{25}$$

In the following paragraphs, we will match this small-scale part of the outer solution to the viscous inner solution. We, therefore, make a Taylor expansion, for small values of θ_{ap},

$$h_{out} = \theta_{ap}x + \frac{1}{2r_0}x^2 + \mathcal{O}(x^3). \tag{26}$$

To express our results in terms of the meniscus rise Δ, we quote the result obtained by James[15] in which the two subregions of the outer meniscus were matched

$$\Delta = r_0\left[\ln\left(\frac{4}{r_0(1+\sin\theta_{ap})}\right) - c\right], \tag{27}$$

where c is Euler's constant (0.57721…).

C. Matching

We are now in a position to perform the matching between inner and outer solutions. First, we write the inner solution in terms of the original variables,

$$h_{\text{in}}(x) = \delta^{1/3}\left[\frac{\kappa_y\theta_e^2x^2}{6\lambda} + b_y\theta_e x + \mathcal{O}(1)\right]. \tag{28}$$

Once more, we separately discuss the limits of large and small fiber radii.

1. Large fiber radius: $r_0 \gg 1$

Comparing the inner solution Eq. (28) to the outer solution Eqs. (19) and (24), one finds the matching conditions

$$\theta_{ap} = \delta^{1/3}b_y\theta_e, \tag{29}$$

$$2-\theta_{ap} = \sqrt{2}\delta^{1/3}\frac{\kappa_y\theta_e^2}{3\lambda}. \tag{30}$$

Adding these two conditions leads to an equation for s_1 as a function of δ

$$\frac{2/\theta_e}{\delta^{1/3}} + \frac{2^{2/3}Ai'(s_1)}{Ai(s_1)} = \frac{2^{1/6}\exp[-1/(3\delta)]}{3\pi Ai^2(s_1)\lambda/\theta_e}. \tag{31}$$

Once s_1 is known, one can compute the apparent contact angle

$$\frac{\theta_{ap}}{\theta_e} = \frac{-2^{2/3}\delta^{1/3}Ai'(s_1)}{Ai(s_1)}. \tag{32}$$

A typical result for θ_{ap} as a function of Ca is shown in Fig. 3 (solid curve: $r_0 = 1000$). At vanishing speed, one recovers the equilibrium contact angle ($\theta_e = 0.1$ in this example). The apparent contact angle decreases for increasing speed and tends to $\theta_{ap} = 0$ at a critical value Ca_c. The prediction from the matching compares very well to direct numerical solution of the problem, which will be discussed in Sec. II C 2 (solid squares). Of course, it is also possible to determine the critical speed directly from Eq. (31), as shown in Ref. 13. The critical value δ_c is obtained when the Airy function takes its global maximum, $Ai'(s_1) = 0$, corresponding to $s_{\max} = -1.088\cdots$. This gives a critical speed

$$\delta_c = \frac{1}{3}\left[\ln\left(\frac{\delta_c^{1/3}\theta_e^2}{2^{5/6}3\pi(Ai(s_{\max}))^2\lambda}\right)\right]^{-1}. \tag{33}$$

Note that $\delta = 3\text{Ca}/\theta_e^3$ and $Ai(s_{max}) = 0.53566\ldots$. Physically, this corresponds to a vanishing apparent contact angle, as can be seen from Eq. (32) since $Ai'(s_1) = 0$. Indeed, this confirms the conjecture by Deryaguin and Levi[11] that the maximum speed is attained when $\theta_{ap} = 0$.

2. Small fiber radius: $r_0 \ll 1$

We now perform a similar analysis for thin fibers by using the outer solution (26), which was never worked out previously. Comparing this to the inner solution (28), one finds the matching conditions

$$\theta_{ap} = \delta^{1/3}b_y\theta_e, \tag{34}$$

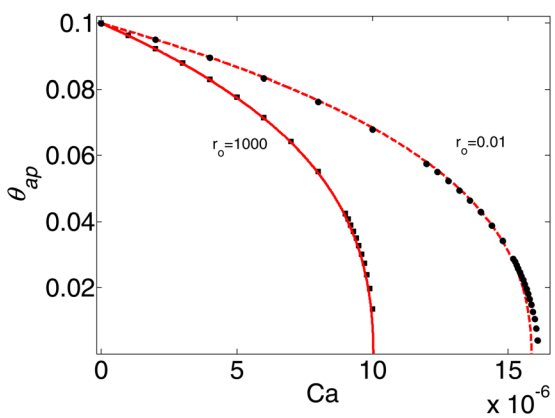

FIG. 3. (Color online) Apparent contact angle θ_{ap} versus Ca ($\lambda = 10^{-8}$, $\theta_e = 0.1$ radian) for large radius ($r_0 = 1000$) and small radius ($r_0 = 0.01$). Curves: result from asymptotic matching, solid curve: $r_0 = 1000$ and dashed curve: $r_0 = 0.01$. Symbols: numerical result, squares: $r_0 = 1000$ and circles: $r_0 = 0.01$.

$$\frac{1}{r_0} = \delta^{1/3}\frac{\kappa_y \theta_e^2}{3\lambda}. \tag{35}$$

The parameter s_1 can be solved as function of δ from Eq. (35). More explicitly, we can write Eq. (35) as

$$\frac{2/\theta_e}{\delta^{1/3}} = \frac{2^{2/3} r_0 \exp[-1/(3\delta)]}{3\pi Ai^2(s_1)\lambda/\theta_e}. \tag{36}$$

The apparent contact angle follows from Eq. (34). Since this condition is the same for both small fiber radius and large fiber radius, the explicit form of θ_{ap} is also given by Eq. (32).

Once again, solutions of the matching conditions cease to exist at a critical speed, which occurs when the Airy function takes it global maximum, $Ai'(s_1) = 0$. In perfect analogy to the flat plate case, this corresponds to $\theta_{ap} = 0$. The critical speed is given by

$$\delta_c = \frac{1}{3}\left[\ln\left(\frac{r_0 \delta_c^{1/3}\theta_e^2}{2^{1/3}3\pi(Ai(s_{\max}))^2\lambda}\right)\right]^{-1}. \tag{37}$$

This result has the same structure as Eq. (33), valid for $r_0 \gg 1$. Apart from numerical coefficients, the main difference is that the fiber radius r_0 appears inside the logarithm as the relevant outer length scale; for the flat plate, the outer scale is the capillary length.

This result is further illustrated in Fig. 3 showing θ_{ap} for a radius $r_0 = 10^{-2}$ (dashed curve). The curve is similar to that obtained for a plate of infinite radius, with a vanishing contact angle at the critical point. Note that this critical speed depends weakly (logarithmically) on the fiber radius, in agreement with prediction Eq. (37). In addition, there is also a logarithmic dependence of δ_c on the equilibrium contact angle θ_e. Let us emphasize that the validity of the asymptotic analysis requires λ/θ_e to be small. This means that, strictly speaking, we cannot deal with extremely small values of θ_e.

It is instructive to compare our results with Voinov's formula.[6] The prediction by Voinov for δ_c has the same structure as ours, but the factor inside the logarithm is not precisely specified (a ratio between the macroscopic length scale and the microscopic scale). In fact, the factor reflects the dependence on the specific geometry of the problem, which in our approach is determined by the matching of the inner region and the outer region. Naturally, the inner scale turns out to be the slip length, while the outer scale is the fiber radius or the capillary length. However, Voinov's formula misses details like the factors θ_e, δ_c inside the logarithm. Also the resulting θ_{ap} vs Ca is a bit different from Voinov's formula, as was previously discussed in detail by Eggers for the plate case.[13]

III. NUMERICAL SOLUTION

We now perform a numerical analysis of the fiber withdrawal problem. This will confirm the validity of the asymptotics and extend the results to $r_0 \sim 1$. However, the main added value is that the numerical solution can determine the complete bifurcation diagrams of dewetting for arbitrary r_0. These contain steady state solutions above $\Delta_{\max}$ that serve as transients towards film deposition,[20,30] and thus provide crucial additional information. Below, we first develop a lubrication model that accounts for the axisymmetric nature of the flow. This quantitative correction with respect to the flat plate will turn out important for the bifurcation diagram. We then summarize the numerical results.

A. Lubrication approximation on a fiber

To formulate a hydrodynamic model for the axisymmetric meniscus on a fiber, we consider Stokes equations

$$-\vec{\nabla}p + \eta\nabla^2\vec{U} - \vec{\nabla}\Phi = 0, \tag{38}$$

$$\vec{\nabla}\cdot\vec{U} = 0, \tag{39}$$

where p is the pressure field in the liquid, η is the viscosity of the liquid, $\vec{U}$ is the velocity field in the frame comoving with the fiber, and Φ is the gravitational potential per unit volume in the liquid. Since the meniscus is axisymmetric, the velocity in azimuthal direction is zero. We consider small contact angle, $\theta_e \ll 1$, thus, the flow is mainly in the vertical x direction, namely, the radial component of velocity is much smaller than the vertical component (i.e.$|U_r| \ll |U_x|$). The flow is solved with a no-stress condition at the interface, is located at $r = r_0 + h$, and reads (in the frame of the fiber)

$$\eta\left(\frac{\partial U_r}{\partial x} + \frac{\partial U_x}{\partial r}\right)_{r=r_0+h} \approx \eta\frac{\partial U_x}{\partial r}|_{r=r_0+h} = 0. \tag{40}$$

At the fiber surface, $r = r_0$, we apply a Navier slip boundary condition

$$U_x|_{r=r_0} = \lambda\frac{\partial U_x}{\partial r}|_{r=r_0}. \tag{41}$$

The axial (vertical) component of the velocity field then becomes

$$U_x = \frac{1}{2\eta}\frac{\partial(p+\Phi)}{\partial x} \times\left[\frac{r^2 - r_0^2}{2} - (r_0+h)^2\ln\left(\frac{r}{r_0}\right) - \lambda\left(2h + \frac{h^2}{r_0}\right)\right]. \tag{42}$$

For thin films $h/r_0 \ll 1$, this reduces to the usual parabolic Poiseuille profile but quantitative corrections appear when $h/r_0 \sim 1$.

The lubrication equation is obtained by imposing a zero flux condition in the frame of the reservoir

$$\int_{r_0}^{r_0+h}(U_x + U_0)r dr = 0. \tag{43}$$

With this, Eq. (42) can then be simplified as

$$\frac{\partial(p+\Phi)}{\partial x} = \frac{3\eta U_0 f(d)}{h[h + 3\lambda(1+d/2)f(d)]}, \tag{44}$$

where we introduced $d = h/r_0$ and

$$f(d) = \frac{8d^3(2+d)}{3[4(1+d)^4 \ln(1+d) - d(2+d)(2+6d+3d^2)]}. \tag{45}$$

This function is a correction factor with respect to the flat plate ($d=0$) and has the property $f(0)=1$. Finally, we replace the pressure by the Young-Laplace equation,

$$p - p_0 = -\gamma\kappa, \tag{46}$$

where κ is the curvature of the interface given by Eq. (15). This gives the lubrication equation on a fiber

$$\frac{\partial\kappa}{\partial x} = \frac{3\mathrm{Ca}f(d)}{h[h+3\lambda(1+d/2)f(d)]} - 1. \tag{47}$$

Note that once again all lengths are scaled by the capillary length. For $d = h/r_0 \ll 1$, we recover the usual lubrication equation since $f(0)=1$.

B. Results

1. Critical speed

The above lubrication Eq. (47) is solved numerically with boundary conditions

$$h(0) = 0, \tag{48}$$

$$h'(0) = \theta_e, \tag{49}$$

imposed at the contact line and

$$h'(\Delta) = \infty, \tag{50}$$

$$\kappa(\Delta) = 0, \tag{51}$$

at the reservoir. We varied r_0 and λ and determined the meniscus as a function of Ca.

Figure 4 shows the meniscus rise Δ as a function of Ca on a fiber of radius $r_0 = 10^{-2}$. Different symbols correspond to different values of the slip length. In all cases, we find a critical $\mathrm{Ca_c}$ above which solutions cease to exist. This indeed occurs close to $\Delta_{\max}$ corresponding to a vanishing θ_{ap}, which is indicated by the horizontal dotted line. The curves are the predictions from the matched asymptotics, showing a good agreement with the numerical solutions. In particular, one observes convergence as the slip length is reduced from $\lambda = 10^{-6}$, 10^{-7} to 10^{-8}. This is because the separation of the two length scales λ and r_0 is enhanced, which improves the validity of the matching asymptotic expansion. The same results were previously reported in Fig. 3, expressed in terms of θ_{ap} rather than Δ.

It is interesting to show how the critical speed Ca_c depends on the fiber radius r_0. The numerical results are plotted as squares in Fig. 5. In agreement with the asymptotic analysis, one observes two regimes. At small radii, $r_0 \ll 1$, the critical speed depends logarithmically on the radius. The solid red line is the asymptotic result (37). For large radii, the speed approaches the value of the flat plate (33), indicated as dashed black line. Indeed, the cross-over occurs for fibers with a radius that is comparable to the capillary length $r_0 \sim 1$.

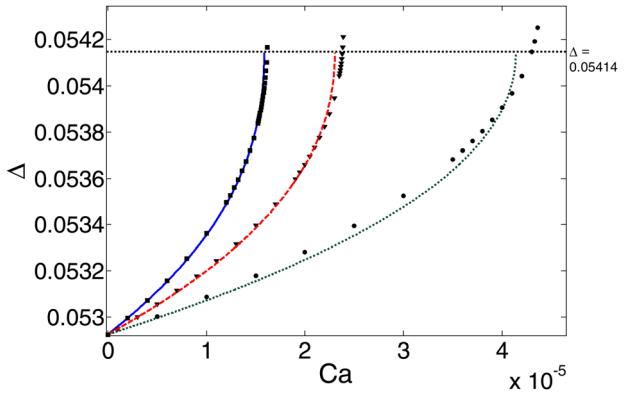

FIG. 4. (Color online) Height of meniscus Δ versus speed for different slip lengths ($r_0 = 10^{-2}$, $\theta_e = 0.1$ radian). Curves are results from asymptotic matching, solid curve (the most left curve): $\lambda = 10^{-8}$, dashed curve: $\lambda = 10^{-7}$, and dotted curve (the most right curve): $\lambda = 10^{-6}$. Symbols are the corresponding numerical results. As the slip length gets smaller, the agreement between numerics and asymptotic matching becomes better. The horizontal dotted line indicates the maximum height of meniscus $\Delta = 0.05414$ calculated by Eq. (27) with $\theta_{ap} = 0$.

2. Meniscus rise: Bifurcation diagram

The results shown in Fig. 4 represent only the lowest branch of solutions of a more complete bifurcation diagram. Indeed, one can identify solutions with Δ extending to arbitrary height above the meniscus, which are all characterized by $\mathrm{Ca} < \mathrm{Ca_c}$. These are summarized in Figs. 6(a)–6(e) for different fiber radii (all curves correspond to $\theta_e = 0.05$ and $\lambda = 10^{-5}$). For $r_0 = 1000$ (Fig. 6(a)), we see after reaching $\mathrm{Ca_c}$, the curve turns back to $\mathrm{Ca} < \mathrm{Ca_c}$ but with solutions of increasing Δ. We refer to these solutions as the second branch, which is known to be unstable.[20] Further upwards, we observe a series of bifurcations to higher branches, oscillating around a characteristic value Ca^*. Typical meniscus profiles are shown in Fig. 6(b)—in order to compare the profiles, we have shifted the positions of the contact line such that the baths collapse. Following the bifurcation diagram, the profiles evolve to a film solution for which the contact

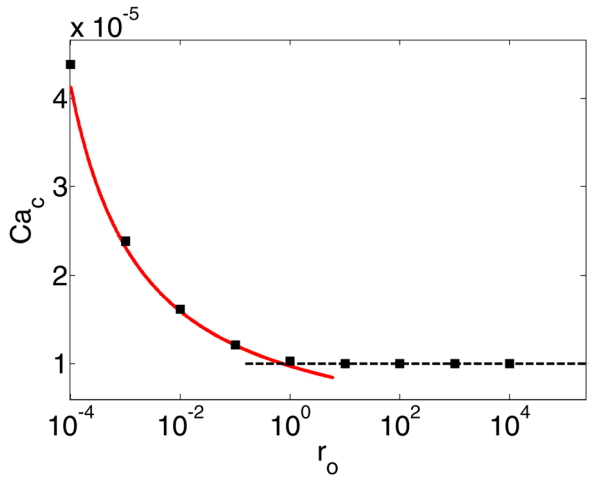

FIG. 5. (Color online) Critical capillary number Ca_c versus fiber radius r_0 ($\theta_e = 0.1$ radian, $\lambda = 10^{-8}$). Squares: numerical results; curve: result from asymptotic matching for small fiber radius [Eq. (37)]; dotted line: result from asymptotic matching for large fiber radius [Eq. (33)].

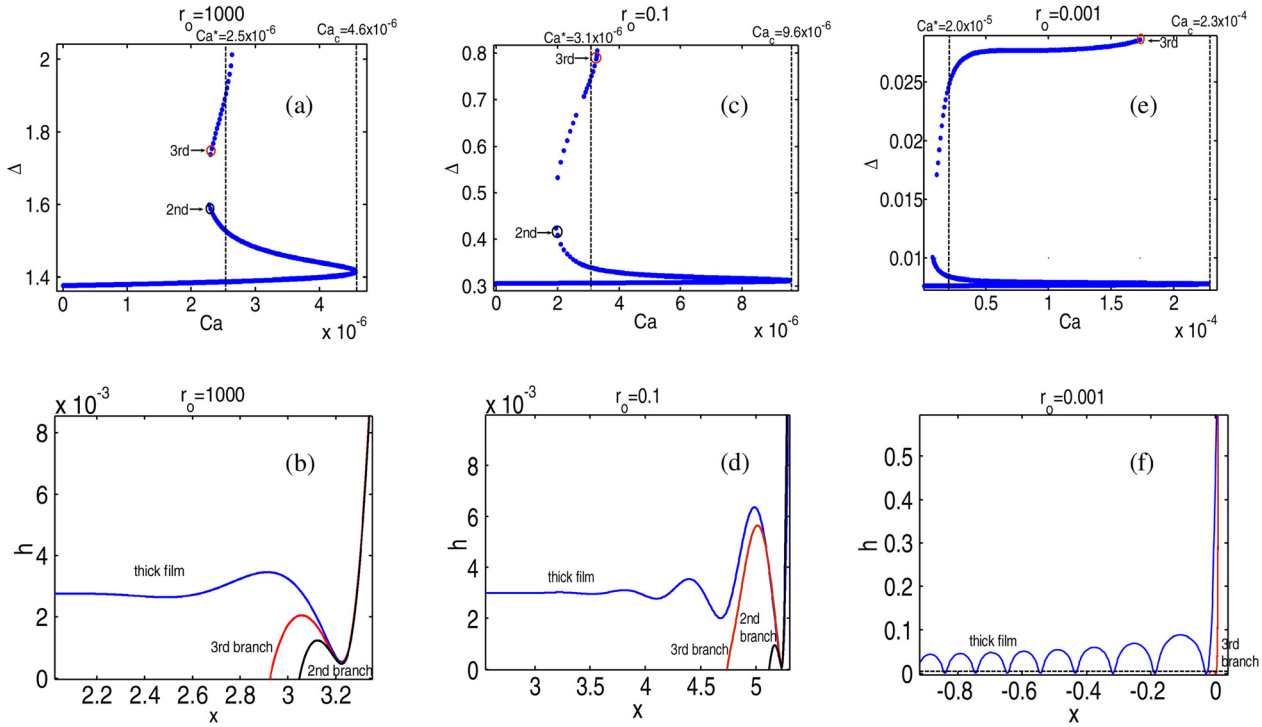

FIG. 6. (Color online) Bifurcation diagrams of steady solutions. Panels (a), (c), and (e): bifurcation diagrams for $r_0 = 1000$, 0.1, and 0.001, respectively. All curves correspond to $\theta_e = 0.05$ and $\lambda = 10^{-5}$. Panels (b), (d), and (f): interface profiles for $r_0 = 1000$, 0.1, and 0.001, respectively. We report profiles from the 2nd branch and 3rd branch, corresponding to solutions indicated in the bifurcation diagram by large circles. The "thick film" solutions correspond to profiles without contact line, or $\Delta \to \infty$, for which we define $\mathrm{Ca} = \mathrm{Ca}^*$. The thickness of the film for $r_0 = 0.001$ is shown by the horizontal line just above x axis in (f).

line has moved to arbitrary height above the meniscus, i.e., $\Delta \to \infty$. This film solution (shown in Fig. 6(b)) is not the Landau-Levich-Deryaguin film, but corresponds to the new class of "thick film" solutions identified in Ref. 5.

We then decrease the fiber radius to $r_0 = 0.1$, as shown in Figs. 6(c) and 6(d). We find that $\mathrm{Ca_c}$ increases almost by a factor 2 with respect to the large radius. By contrast, Ca^* corresponding to the thick film increases only by a small amount. As a result, the values of $\mathrm{Ca_c}$ and Ca^* have become more separated. Also, the corresponding meniscus profiles display more structure. The thick film exhibits much stronger oscillations before joining the reservoir. These trends becomes more dramatic up further decreasing the radius $r_0 = 0.001$ (Figs. 6(e) and 6(d)). The difference between $\mathrm{Ca_c}$ and Ca^* is very pronounced and Δ changes much more dramatically for the 3rd branch solutions. In this sense, the bifurcation diagram has a very different structure from those of large fiber radius. Interestingly, there still exists a thick film solution matching to the bath, but the profile displays many oscillations (Fig. 6(f)). These oscillations decay only very slowly when moving further away from the bath—the asymptotic thickness of the film is indicated by the horizontal line just above x axis. While for the flat plate, the thick film solutions have been observed experimentally,[5] we expect the oscillatory solution obtained for small radii to be unstable and of no physical relevance.

For completeness, we report the values of $\mathrm{Ca_c}$ and Ca^* for different radii in a separate graph (Fig. 7). Note that the theoretical curve for $\mathrm{Ca_c}$ deviates from the numerical results as early as $r_0 \lesssim 10^{-2}$. The reason is that, here, we use a realistic value for the slip length $\lambda = 10^{-5}$ (corresponding to ~ 10 nm), instead of $\lambda = 10^{-8}$ used in Fig. 5. Clearly, the scale separation required for the asymptotic analysis starts to break down when the ratio λ/r_0 is no longer very small.

IV. DISCUSSION

We investigated the steady-state profiles of axisymmetric menisci on a fiber that is withdrawn from a viscous liquid. The main motivation for this work was the mixed experimental observations on the transition to film deposition obtained for

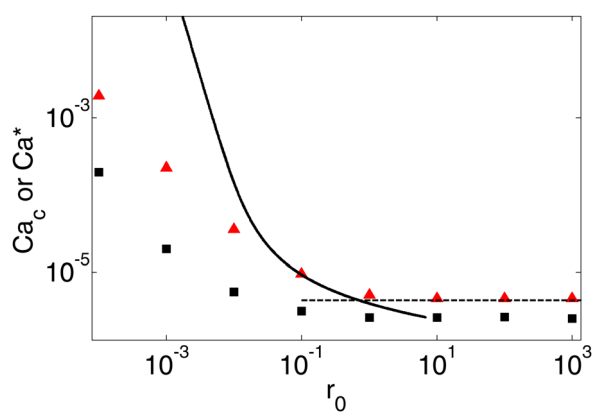

FIG. 7. (Color online) $\mathrm{Ca_c}$ and Ca^* as function of r_0 for the same parameters used in Fig. 6. Triangles: numerical results for $\mathrm{Ca_c}$; squares: numerical results for Ca^*; curve: result for $\mathrm{Ca_c}$ from asymptotic matching for small fiber radius [Eq. (37)]; dotted line: result for $\mathrm{Ca_c}$ from asymptotic matching for large fiber radius [Eq. (33)].

fibers, large cylinders, and plates. Sedev and Petrov[16] found that the maximum steady profile has a meniscus rise identical to a perfectly wetting liquid at equilibrium, suggesting a vanishing apparent contact angle θ_{ap}. Other experiments found that the steady-state solutions disappeared at a nonzero θ_{ap},[17,18] although the critical point could be accessed during transients.[19] Our present calculations show that steady solutions always cease to exist at $\theta_{ap}=0$, independent of the fiber radius. In addition, stability arguments put forward in Refs. 38 and 13 suggest that all solutions of the lowest branch are perfectly stable up to the maximum speed, consistent with a saddle-node bifurcation.[20] In that sense, our results do not provide an explanation why experimentally it is practically impossible to achieve steady menisci closer to $\theta_{ap}=0$. The main effect that was not taken into account in our calculations is contact angle hysteresis due to heterogeneity of the substrate,[39] which was previously suggested to affects the details of the transition.[40] It has remained a challenge, however, to incorporate this into a full hydrodynamic description of moving contact lines. Essentially, one has to modify the boundary condition by imposing a time-dependent microscopic contact angle at the moving contact line.

The bifurcation diagrams calculated in the second part of the paper, however, do provide a new experimental perspective on the dynamics of film deposition. As shown in Ref. 19, such bifurcation diagrams may be probed experimentally as transient states during entrainment. Namely, for $\mathrm{Ca} > \mathrm{Ca}_c$, the evolution of the meniscus exactly follows the bifurcation diagram when plotting Δ versus the *relative* contact line velocity with respect to the solid. For very large fiber radius, the profiles with large capillary rise are smoothly connected to the bath by a film that only displays a small "dimple" close to the bath. These dimple solutions have indeed been observed experimentally when plates are withdrawn with speeds above the critical speed. By contrast, for small fiber radii, these solutions exhibit very strong oscillations (Fig. 6) and we expect these solutions to be very unstable. In that case, another dynamical mode must appear in order to deposit a liquid film—for example, one could think of the classical dewetting rim at the contact line connected to a Landau-Levich film.[41] A further investigation of these transients above the critical speed, in particular for different radii, should give a more complete picture of the forced wetting transition.

ACKNOWLEDGMENTS

We are grateful to Jens Eggers and Bruno Andreotti for discussions and support. T.S.C. acknowledges financial support by the FP7 Marie Curie Initial Training Network "Surface Physics for Advanced Manufacturing" Project No. ITN 215723.

[1]D. Quéré, "Fluid coating on a fiber," Annu Rev. Fluid Mech. **31**, 347 (1999).
[2]S. J. Weinstein and K. J. Ruschak, "Coating flows," Annu. Rev. Fluid Mech. **36**, 29 (2004).
[3]L. D. Landau and B. V. Levich, "Dragging of a liquid by a moving plate," Acta Physicochim. USSR **17**, 42 (1942).
[4]B. V. Deryaguin, "On the thickness of a layer of liquid remaining on the walls of vessels after their emptying, and the theory of the application of photoemulsion after coating on the cine film," Acta Physicochim. USSR **20**, 349 (1943).
[5]J. H. Snoeijer, J. Ziegler, B. Andreotti, M. Fermigier, and J. Eggers, "Thick films coating a plate withdrawn from a bath," Phys. Rev. Lett. **100**, 244502 (2008).
[6]O. V. Voinov, "Hydrodynamics of wetting [English translation]," Fluid Dynam. **11**, 714 (1976).
[7]R. G. Cox, "The dynamics of the spreading of liquids on a solid surface. Part 1. Viscous flow," J. Fluid Mech. **168**, 169 (1986).
[8]P.-G. de Gennes, "Deposition of langmuir-blodget layers," Colloid Polym. Sci. **264**, 463 (1986).
[9]L. W. Schwartz, D. Roux, and J. J. Cooper-White, "On the shapes of droplets that are sliding on a vertical wall," Phys. D **209**, 236 (2005).
[10]D. Bonn, J. Eggers, J. Indekeu, J. Meunier, and E. Rolley, "Wetting and spreading," Rev. Mod. Phys. **81**, 739 (2009).
[11]B. V. Deryaguin and S. M. Levi, *Film Coating Theory* (Focal, London, 1964).
[12]J. Eggers, "Hydrodynamic theory of forced dewetting," Phys. Rev. Lett. **93**, 094502 (2004).
[13]J. Eggers, "Existence of receding and advancing contact lines," Phys. Fluids **17**, 082106 (2005).
[14]L. D. Landau and E. M. Lifshitz, *Fluid Mechanics* (Oxford, Pergamon, 1984).
[15]D. F. James, "The meniscus on the outside of a small circular cylinder," J. Fluid Mech. **63**, 657 (1973).
[16]R. V. Sedev and J. G. Petrov, "The critical condition for transition from steady wetting to film entrainment," Colloids Surf. **53**, 147 (1991).
[17]M. Maleki, E. Reyssat, D. Quéré, and R. Golestanian, "On the Landau-Levich transition," Langmuir **23**, 10116 (2007).
[18]J. H. Snoeijer, G. Delon, M. Fermigier, and B. Andreotti, "Avoided critical behavior in dynamically forced wetting," Phys. Rev. Lett. **96**, 174504 (2006).
[19]G. Delon, M. Fermigier, J. H. Snoeijer, and B. Andreotti, "Relaxation of a dewetting contact line. Part 2. Experiments," J. Fluid Mech. **604**, 55 (2008).
[20]J. H. Snoeijer, B. Andreotti, G. Delon, and M. Fermigier, "Relaxation of a dewetting contact line. Part 1. A full-scale hydrodynamic calculation," J. Fluid Mech. **579**, 63 (2007).
[21]T. D. Blake and K. J. Ruschak, "A maximum speed of wetting," Nature **282**, 489 (1979).
[22]C. Duez, C. Ybert, C. Clanet, and L. Bocquet, "Making a splash with water repellency," Nature Phys. **3**, 180 (2007).
[23]K. G. Winkels, I. R. Peters, F. Evangelista, M. Riepen, A. Daerr, L. Limat, and J. Snoeijer, "Receding contact lines: From sliding drops to immersion lithography," Eur. Phys. J. Spec. Top. **192**, 195 (2011).
[24]J. H. Burnett, S. G. Kaplana, E. L. Shirleya, P. Tompkins, and J. E. Webb, "High-index materials for 193 nm immersion lithography," in *Proceedings of SPIE 5754, Optical Microlithography XVIII*, edited by B. W. Smith (SPIE, Bellingham, WA, 2005), Vol. 5754.
[25]T. Podgorski, J. M. Flesselles, and L. Limat, "Corners, cusps, and pearls in running drops," Phys. Rev. Lett. **87**, 036102(1) (2001).
[26]U. Thiele, K. Neuffer, M. Bestehorn, Y. Pomeau, and M. G. Velarde, "Sliding drops on an inclined plane," Colloid Surf. A **206**, 87 (2002).
[27]L. Limat and H. A. Stone, "Three-dimensional lubrication model of a contact line corner singularity," Europhys. Lett. **65**, 365 (2004).
[28]N. Le Grand, A. Daerr, and L. Limat, "Shape and motion of drops sliding down an inclined plane," J. Fluid Mech. **541**, 293 (2005).
[29]J. Snoeijer, N. Le Grand, L. Limat, H. A. Stone, and J. Eggers, "Cornered drop and rivulets," Phys. Fluids **19**, 042104 (2007).
[30]J. Ziegler, J. H. Snoeijer, and J. Eggers, "Film transitions of receding contact lines," Eur. Phys. J. Spec. Top. **166**, 177 (2009).
[31]C. Huh and L. E. Scriven, "Hydrodynamic model of steady movement of a solid/liquid/fluid contact line," J. Colloid Interface Sci. **35**, 85 (1971).
[32]L. M. Hocking, "The spreading of a thin drop by gravity and capillarity," Q. J. Mech. Appl. Math. **36**, 55 (1983).
[33]E. Lauga, M. P. Brenner, and H. A. Stone, "Microfluidics: the no-slip boundary condition," in *Springer Handbook of Experimental Fluid Mechnaics*, edited by C. Tropea, J. F. Foss, and A. Yarin (Springer, New York, 2008), pp. 1219–1240.
[34]C. Cottin-Bizonne, B. Cross, A. Steinberger, and E. Charlaix, "Boundary slip on smooth hydrophobic surfaces: Intrinsic effets and possible artifacts," Phys. Rev. Lett. **94**, 056102 (2005).
[35]A. Oron, S. H. Davis, and S. G. Bankoff, "Long-scale evolution of thin liquid films," Rev. Mod. Phys. **69**, 931 (1997).

[36]B. R. Duffy and S. K. Wilson, "A third-order differential equation arising in thin-film flows and relevant to Tanner's Law," Appl. Math. Lett. **10**, 63 (1997).
[37]M. Abramowitz and I. A. Stegun, *Handbook of Mathematical Functions* (Dover, New York, 1968).
[38]R. Golestanian and E. Raphaël, "Roughening transition in a moving contact line," Phys. Rev. E **67**, 031603 (2003).
[39]J.-F. Joanny and P.-G. de Gennes, "Competition between wetting and adverse macroscopic forces [in French]," C. R. Acad. Sci., Ser. II **299**, 605 (1984).
[40]R. Golestanian and E. Raphaël, "Relaxation of a moving contact line and the Landau-Levich effect," Europhys. Lett. **55**, 228 (2001).
[41]C. Redon, F. Brochard-Wyart, and F. Rondelez, "Dynamics of dewetting," Phys. Rev. Lett. **66**, 715 (1991).